Geophysical Research Letters

RESEARCH LETTER
10.1029/2020GL088913

Special Section:
The COVID-19 Pandemic: Linking Health, Society and Environment

Limited Regional Aerosol and Cloud Microphysical Changes Despite Unprecedented Decline in Nitrogen Oxide Pollution During the February 2020 COVID-19 Shutdown in China

Michael S. Diamond[1] **and Robert Wood**[1]

[1]Department of Atmospheric Sciences, University of Washington, Seattle, WA, USA

Abstract Following the emergence of a novel coronavirus in Wuhan, China instituted shutdown measures starting in late January and continuing into February 2020 to arrest the spread of disease. This resulted in a sharp economic contraction unparalleled in recent Chinese history. Satellite retrievals show that nitrogen dioxide pollution declined by an unprecedented amount (~50% regionally) from its expected unperturbed value, but regional-scale column aerosol loadings and cloud microphysical properties were not detectably affected. The disparate impact is tied to differential economic impacts of the shutdown, in which transportation, a disproportionate source of nitrogen oxide emissions, underwent drastic declines (~90% reductions in passenger traffic), whereas industry and power generation, responsible for >90% of particulate emissions, were relatively less affected (~20% reductions in electricity and thermal power generation). A combination of anomalously warm and humid meteorological conditions and complex chemical interactions further decreased nitrogen dioxide concentrations but likely enhanced secondary aerosol formation.

Plain Language Summary To slow the spread of COVID-19, China implemented strict policies limiting travel and public gatherings in February 2020, resulting in a pronounced economic decline. Satellite measurements show that levels of nitrogen oxides, gases that are a major component of air pollution, were substantially lower than what we would normally expect for February. Surprisingly, however, we did not observe any similar changes in airborne particles (another major component of air pollution) or in the size of cloud droplets (which is partly determined by the abundance of airborne particles). This is important because airborne particles, in addition to harming human health, affect the climate by changing how much sunlight is absorbed on Earth versus reflected back into space. The transportation sector of the economy was hit particularly hard by the coronavirus shutdown, but heavy industries and power plants were relatively less affected. Transportation is a major source of nitrogen oxides but not of airborne particles or their chemical precursors, which are mostly emitted by industry and power plants. The shutdown's much larger effect on transportation than on industry or power plants, along with changes in weather and chemical interactions, help explain the differences we see in the different types of air pollution.

Key Points:
- Rapid economic collapse in February 2020 due to the COVID-19 pandemic and partial recovery in March 2020 are unique in recent Chinese history
- Regional decline in NO_2 pollution is unprecedented in the satellite record, but no change in aerosol or cloud properties is detected
- Different economic impacts by sector, meteorology, and complex chemical interactions help explain differences in NO_x and aerosol response

Supporting Information:
- Supporting Information S1

Correspondence to:
M. S. Diamond,
diamond2@uw.edu

Citation:
Diamond, M. S., & Wood, R. (2020). Limited regional aerosol and cloud microphysical changes despite unprecedented decline in nitrogen oxide pollution during the February 2020 COVID-19 shutdown in China. *Geophysical Research Letters*, *47*, e2020GL088913. https://doi.org/10.1029/2020GL088913

Received 16 MAY 2020
Accepted 31 JUL 2020
Accepted article online 19 AUG 2020

1. Introduction

1.1. Emergence of a Novel Coronavirus and the Societal Response to the Resulting COVID-19 Pandemic

In late December 2019, cases of a pneumonia of unknown cause were reported in the city of Wuhan. By January 2020, the pathogen responsible—a novel zoonotic coronavirus—had already spread throughout China and other nations including Japan, South Korea, and the United States (C. Wang, et al., 2020). To arrest the spread of COVID-19 (the disease caused by the novel coronavirus), a series of strict restrictions on travel and other activities were adapted across China, slowing the spread of the epidemic in China even as the disease became a global pandemic (Maier & Brockmann, 2020; Tian et al., 2020).

Unsurprisingly, this socioeconomic "shutdown" had a catastrophic effect on the Chinese economy. Figure 1 shows the purchasing managers' index (PMI) for both manufacturing and nonmanufacturing sectors as

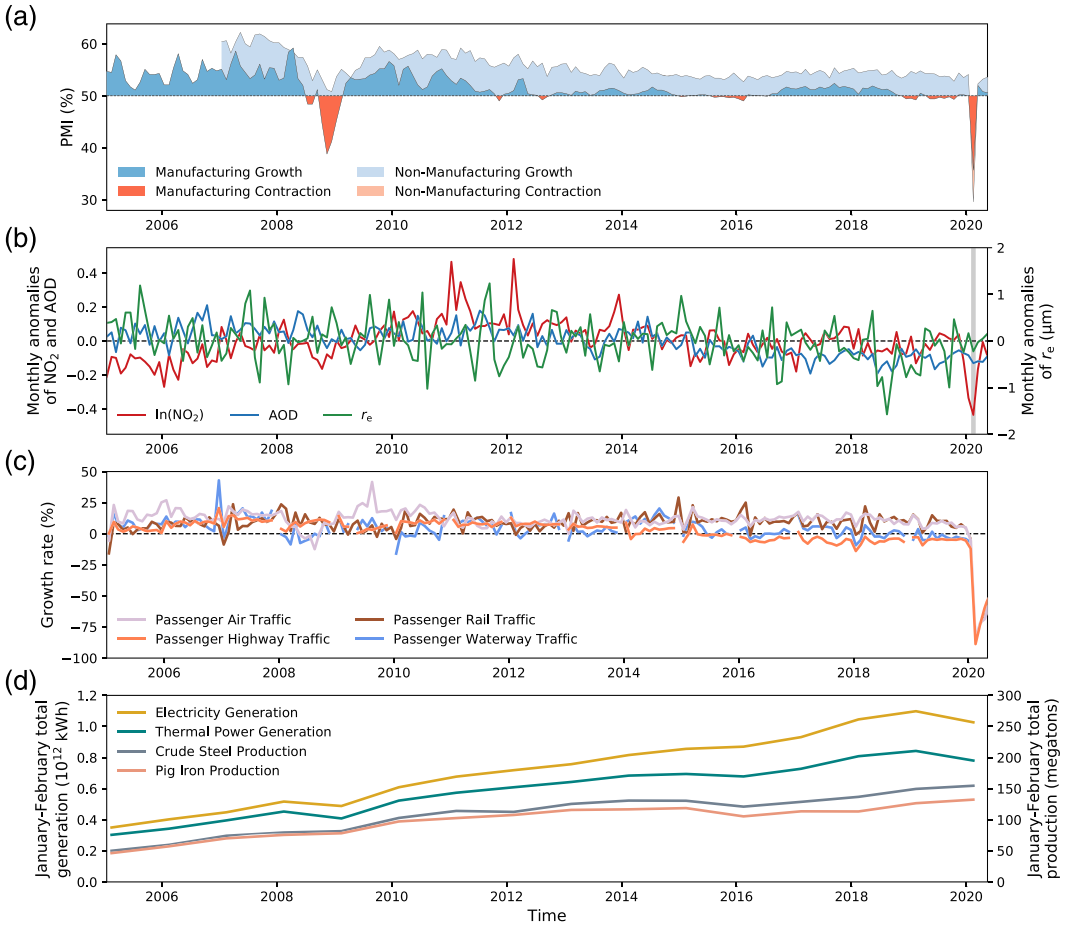

Figure 1. Economic and environmental indicators from January 2005 to May 2020. (a) China's purchasing managers' index. Economic growth is indicated by blue shading and contraction by red shading (darker colors signify the manufacturing and lighter colors the nonmanufacturing sectors). (b) Monthly anomalies of $\ln(NO_2)$ (red) and aerosol optical depth (blue) averaged over eastern China and cloud droplet effective radius (green) averaged over the East China Sea. February 2020 is highlighted in gray shading. (c) Year-on-year growth rate of passenger transportation by month. (d) Combined January–February totals of power generation and some heavy industries.

reported by the National Bureau of Statistics of China. The PMI is a survey-based estimate of economic activity, with values above 50% corresponding to growth and below to contraction (Harris, 1991). February 2020 stands out sharply, featuring a decline in manufacturing PMI deeper than any point during the aftermath of the 2008 financial crisis and the only period of contraction in nonmanufacturing PMI since records for that index began in 2007, followed by a rapid recovery.

1.2. Anthropogenic Drivers of Recent Pollution Changes

Nitrogen oxides ($NO_x \equiv NO + NO_2$) are reactive, short-lived gases that are a major constituent of air pollution harmful to human health (Atkinson et al., 2018). Due to rapid cycling between NO and NO_2 in the atmosphere, changes in NO_2 indicate changes in NO_x overall. Tiny particles suspended in the air (aerosol) are another major component of air pollution. Particulate matter with aerodynamic diameters of 2.5 μm or smaller ($PM_{2.5}$) is known to have severe health impacts, with some estimates of global excess mortality due to outdoor $PM_{2.5}$ approaching 10 million deaths annually (Burnett et al., 2018).

In addition to their relevance for public health, aerosol particles influence the climate through absorbing and scattering sunlight and by changing the optical properties of other components of the Earth

system like snow, ice, and clouds. In particular, gaps in our knowledge about the interactions between clouds and aerosol particles represent the largest source of uncertainty in present-day anthropogenic radiative forcing in the most recent Intergovernmental Panel on Climate Change (IPCC) assessment (Myhre et al., 2013). Aerosol particles can serve as cloud condensation nuclei (CCN) upon which liquid-phase cloud droplets may form. Increasing CCN increases the number of cloud droplets and (for the same amount of liquid water) decreases their size, increasing cloud reflectivity (Twomey, 1977). Macrophysical cloud adjustments to these microphysical changes can either enhance or offset this "Twomey effect" (Ackerman et al., 2004; Albrecht, 1989). Aerosol also influences mixed-phase and ice cloud properties, although the climatic effects of these changes are even less certain (Storelvmo, 2017).

Determining whether observed cloud changes are attributable to aerosol or meteorological factors is a major challenge (Gryspeerdt et al., 2016; Stevens & Feingold, 2009). To better constrain causality, there has been a growing literature on "natural experiments" like volcanic eruptions and inadvertent anthropogenic modifications like ship tracks (Malavelle et al., 2017; Toll et al., 2019). A clear signal in aerosol and cloud properties due to the February 2020 shutdown would be of great interest to those working to constrain the magnitude of aerosol-cloud interactions.

Both long-term changes in air pollution and aerosol-cloud interactions over China and short-term changes attributable to individual events have been analyzed extensively. Increasing aerosol and cloud droplet number concentrations were associated with China's rapid economic growth between the 1980s and the 2000s (Bennartz et al., 2011). Over the past decade, however, sulfate aerosol and cloud droplet number concentrations have declined (McCoy et al., 2018). Recent declines in pollutants like $PM_{2.5}$ and NO_2 have been driven by increasingly stringent environmental policies (Jin et al., 2016) including goals set by the eleventh (2006–2010) and twelfth (2011–2015) Five-Year Plans (de Foy et al., 2016; Liu et al., 2016; van der A et al., 2017), the 2013 Air Pollution Prevention and Control Action Plan (A. Ding et al., 2019; Silver et al., 2018; Zhai et al., 2019; Zhang et al., 2019; B. Zheng et al., 2018; Y. Zheng et al., 2017), and the 2018 Three-Year Action Plan for Winning the Blue Sky Defense Battle. Ephemeral pollution decreases have also been associated with high-profile events like the 2008 Olympics and Paralympics in Beijing (Cermak & Knutti, 2009; Witte et al., 2009), the 2010 World Expo in Shanghai (Hao et al., 2011), and the 2014 Youth Olympic Games in Nanjing (J. Ding et al., 2015).

Research has already begun on the environmental consequences of COVID-19. Carbon dioxide emissions have significantly declined due to shutdown measures worldwide (Le Quéré et al., 2020). Strong declines in NO_2 have been observed in Europe, China, South Korea, and the United States (Bauwens et al., 2020; Liu et al., 2020); however, emissions reductions related to the early Chinese shutdown were insufficient to avoid bad haze episodes in several cities (Chang et al., 2020; X. Huang et al., 2020; Le et al., 2020; P. Wang et al., 2020) and benefits from decreasing NO_x and $PM_{2.5}$ may be offset by related increases in ozone (X. Huang, Ding, Gao, et al., 2020; Shi & Brasseur, 2020). We add to this work by examining regional-scale NO_x changes alongside possible aerosol and cloud changes in the context of the 2005–2020 satellite record and by drawing upon meteorological, economic, and emissions data to help explain the differences we observe between pollutants during China's February 2020 shutdown.

2. Data

We analyze monthly mean pollution and cloud properties from January 2005 to May 2020 using National Aeronautics and Space Administration's (NASA's) "A-train" satellite constellation (local overpass times ~13:30). NO_2 and SO_2 data are from the Ozone Monitoring Instrument (OMI) on Aura (Levelt et al., 2018; Schoeberl et al., 2006) and aerosol optical depth (AOD), liquid-phase cloud droplet effective radius (r_e), single-scatter albedo (ω_0), and Ångström exponent (α) data are from the Moderate Resolution Imaging Spectroradiometer (MODIS) on Aqua (Parkinson, 2003). For OMI, we compute monthly averages using NASA's standard daily 0.25° by 0.25° gridded products for NO_2 tropospheric column retrievals screened for cloud fractions below 30% (Krotkov et al., 2017, 2019) and planetary boundary layer (PBL) SO_2 (Krotkov et al., 2015). For MODIS, we use standard monthly 1.0° by 1.0° gridded Collection 6.1 products for AOD at 550 nm, liquid r_e retrieved using the near-infrared 2.1 μm channel and a visible channel (Hubanks et al., 2019; Platnick et al., 2017), and ω_0 at 470 nm and α from the Deep Blue algorithm

(Hsu et al., 2013; Sayer et al., 2019). More information about the satellite retrievals are provided in the supporting information.

Two-meter air temperature and specific humidity and 10-m winds are from the Modern-Era Retrospective analysis for Research and Applications, Version 2 (MERRA-2) product (Gelaro et al., 2017) and are bilinearly interpolated to OMI/MODIS grids as needed.

Monthly economic statistics are compiled from the National Bureau of Statistics of China (NBSC). Emissions of NO_x, $PM_{2.5}$, and SO_2 in 2015 broken down by economic sector (IPCC, 2006) are provided by the Emissions Database for Global Atmospheric Research (EDGAR), version 5.0 (Crippa et al., 2018, 2020).

3. Pollution Changes During the February 2020 Shutdown

3.1. Regression Model

Monthly anomalies of $\ln(NO_2)$, AOD, and r_e are shown in Figure 1b. We average the $\ln(NO_2)$ and AOD values over a region (20–42°N, 108–125°E) encompassing the eastern provinces of the People's Republic of China, Hong Kong, and Taiwan. We average r_e over a region (23–35°N, 122–130°E) in the East China Sea in which previous studies have examined aerosol-related cloud microphysical trends (Bennartz et al., 2011; McCoy et al., 2018). Perhaps surprisingly, no clear perturbation can be seen in the cloud or aerosol fields in February 2020, and it is not clear that the apparent decline in $\ln(NO_2)$ is statistically distinguishable from other variations not associated with such an abrupt socioeconomic upheaval. Simply comparing observed pollution levels in 2020 to values from previous years or a long-term average can be misleading due to seasonal cycles and trends in emissions and/or concentrations. For example, one may expect February 2020 pollution levels to have been below the 2015–2019 mean even without any coronavirus-related disturbance due to policy-related trends.

To address these issues, we employ an ordinary least squares linear regression model (Pedregosa et al., 2011) to better estimate what monthly mean air pollution and cloud properties should have been in the absence of coronavirus-related perturbations:

$$Y(t,\phi,\lambda) = c_0(\phi,\lambda) + c_{\text{pre}}(\phi,\lambda)P_{\text{pre}}(t) + c_{\text{post}}(\phi,\lambda)P_{\text{post}}(t) + c_{\text{CNY}}(\phi,\lambda)H_{\text{CNY}}(t) + c_{\cos}(\phi,\lambda)S_{\cos}(t) + c_{\sin}(\phi,\lambda)S_{\sin}(t), \quad (1)$$

where Y is the geophysical variable of interest—$\ln(NO_2)$, AOD, or r_e—as a function of time (t, in months since January 2005) estimated independently at each grid box of latitude ϕ and longitude λ and the regressors P, H, and S are defined as follows. Each constant c and the intercept c_0 are calculated independently at each grid box. We use the natural logarithm of NO_2 rather than its absolute value for the regression because NO_2 is distributed log-normally in space (de Foy et al., 2016) and later analyses involve taking spatial averages. The model is fit based on data from January 2005 to December 2019 and is used to predict the expected values for January–May 2020.

We define the regressors P_{pre} and P_{post} as the trend in terms of months preceding or following January 2013, respectively. January 2013 was chosen as the policy "turning point" due to the severe haze events that occurred early that year (R. Huang et al., 2014; G. Zheng et al., 2015) that contributed to the creation of the ambitious Air Pollution Prevention and Control Action Plan in September 2013 (Jin et al., 2016).

Next, the regressor H_{CNY} refers to whether the Chinese New Year holiday and related festivities (Jiang et al., 2015; Tan et al., 2009) occurred during time t. When Chinese Lunar New Year begins in February, H_{CNY} is assigned a value of 1. When the holiday begins in late January with festivities lasting into early February, H_{CNY} is assigned a value based on the fraction of the 10 days following the Lunar New Year occurring in each month. H_{CNY} is set to zero all other times.

Finally, the regressors $S_{\cos}$ and $S_{\sin}$ refer to idealized seasonal cycles, represented as two annual Fourier modes:

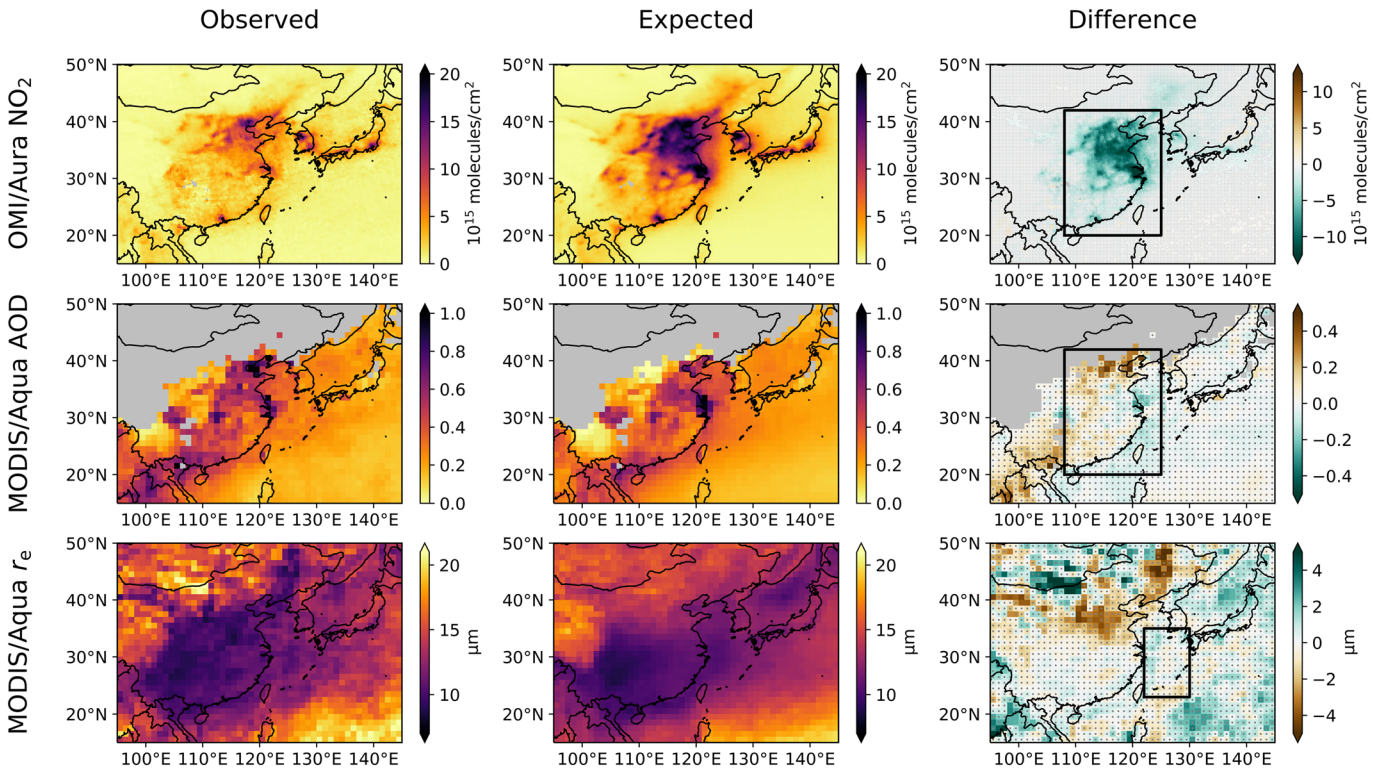

Figure 2. Change in pollution over China for February 2020. (left column) Observed values, (middle column) estimated values, and (right column) their difference are shown for (top row) NO_2, (middle row) AOD, and (bottom row) r_e. Shading is such that lighter (left and middle columns) and greener (right column) colors align with what would be expected for less pollution. Areas without valid data are shaded in gray. Gray stippling indicates absolute differences below $2\varepsilon_{RMS}$. Black boxes in the right column indicate areas used for the regional averages.

$$S_{\cos}(t) = \cos\left(2\pi\frac{m(t)-1}{12}\right), \tag{2}$$

$$S_{\sin}(t) = \sin\left(2\pi\frac{m(t)-1}{12}\right), \tag{3}$$

where m refers to the calendar month (January = 1) at time t.

Supporting information Figure S1 shows the value of each regressor as a function of time; Figure S2 shows maps of the coefficient of determination (R^2), root-mean-square (RMS) error (ε_{RMS}), and number of samples used to fit the regression (N); and Figures S3–S5 show maps of the intercept and regression coefficients for $\ln(NO_2)$, AOD, and r_e, respectively.

3.2. Results

Maps of the observed (retrieved) and expected (regression) values of NO_2, AOD, and r_e for February 2020, along with the difference between the observed and expected values, are shown in Figure 2. (NO_2 values are converted into their absolute values for the sake of presentation.) There is a readily apparent decline in NO_2, in some places rivaling the magnitude of the total tropospheric column, consistent with the results of Bauwens et al. (2020). However, there are no consistent differences in either the aerosol loading or cloud microphysics on a regional scale. Furthermore, regions with the largest discrepancies in the cloud fields tend to be those with the lowest explained variance (Figure S2). The lack of a regional AOD decline is in apparent conflict with some previous results (X. Huang, Ding, Gao, et al., 2020; Le et al., 2020; Shi & Brasseur, 2020), although it should be noted that the quantities of interest (regional-scale column aerosol loading versus surface $PM_{2.5}$ at specific stations) are different. There does appear to be an increase in AOD surrounding Beijing, which is consistent with some previous results (X. Huang, Ding, Gao, et al., 2020; Le et al., 2020). The only area with what appears to be a coherent decline in AOD occurs around Shanghai, although even

that city experienced relatively high levels of surface $PM_{2.5}$ in two events earlier in the month (Chang et al., 2020).

To look at the differences between the observed and estimated values in greater historical perspective, we average the observed and estimated $\ln(NO_2)$, AOD, and r_e values over the same regions used in Figure 1b. Results are displayed in Figure 3, with the root-mean-square (RMS) error in this case calculated using the differences between the spatially averaged observed and expected values from January 2005 to December 2019. Like the PMI indices, $\ln(NO_2)$ shows a pronounced and unprecedented decline in February 2020 followed by a rapid recovery. In contrast, AOD and r_e values during 2020 are not perceptibly distinct from the 2005–2019 record.

Sulfate aerosols, which can form via the oxidation of SO_2 in the atmosphere, are a major source of cloud condensation nuclei. PBL SO_2 as retrieved by OMI is noisier than the tropospheric column NO_2 retrievals and can be affected by factors like elevated volcanic plumes, although previous analyses have successfully analyzed regional-scale trends to gain insight into long-term pollution changes (Krotkov et al., 2016; McCoy et al., 2018). Figure S6 shows PBL SO_2 averaged over eastern Asia excluding major Northern Hemisphere volcanic eruptions. SO_2 levels in February 2020 are in line with the decreasing trend since 2013 and are slightly above the previous year's values, consistent with the minimal change in cloud and aerosol properties.

3.3. Detectability

The differences between our model's expectations and the observations can be due to emissions changes not captured in our broad policy-related trend terms or other factors such as meteorological variability. Thus, for a given emissions reduction, we may not be able to reliably detect that reduction given other fluctuations.

We estimate the probability of detection, defined as the probability that we would observe a regionally averaged change exceeding a given threshold, as follows. For emissions reductions up to 90%, we adjust the expected value by a proportional amount for NO_2 and AOD and then generate a spread using a normal distribution fit with the adjusted expectation and RMS error (Figures 3b, 3d, and 3f). The fraction laying below the threshold is the probability of detection. This method assumes that concentrations/optical properties decline proportionally to emissions, which neglects the idea that not all emissions are anthropogenic; that there may be complex interactions between emissions and concentrations; and that optical properties may not vary linearly with aerosol concentration (especially if the mix of sources changes) but should still provide useful results assuming that natural emissions are small compared to the anthropogenic emissions and if interpreted cautiously. A similar method is employed for r_e, taking into account the more indirect relationship between aerosol and cloud properties by estimating the increase in droplet size for a given reduction in aerosol number (N_a) as

$$\delta\ln(r_e) \approx \delta\ln(N_a)\left(\frac{\delta\ln(N_d)}{\delta\ln(N_a)}\right)\left(\frac{\delta\ln(r_e)}{\delta\ln(N_d)}\right) \approx -\beta\frac{\delta\ln(N_a)}{3}, \tag{4}$$

where N_d is the cloud droplet number concentration, β is the log-log sensitivity of N_d to aerosol changes, and the factor of $-1/3$ relating r_e and N_d changes assumes liquid water path changes are negligible. Because the β parameter is highly uncertain, we bound plausible r_e responses by making separate estimates for low and high sensitivities of 0.3 and 0.8, respectively (Bellouin et al., 2020).

Figure S7 shows the probability of detection for $\ln(NO_2)$, AOD, and both bounded estimates for r_e for detection thresholds of decreases (NO_2 and AOD) or increases (r_e) of one, two, and three RMS errors of the (unadjusted) expected value for February 2020. If emissions were reduced by greater than 80%, there is a very large probability that we would have detected changes in all three variables at the strictest ($3\varepsilon_{RMS}$) threshold (unless the clouds have very low susceptibility to aerosol), whereas if emissions were reduced by 20% or less, we would be unlikely to detect changes in any of the variables at the strictest threshold and only have even odds of detecting aerosol or cloud changes at the most lenient threshold ($1\varepsilon_{RMS}$). For a 50% emissions reduction, we would be very likely to detect a NO_2 change at any threshold, whereas detection of changes in AOD or r_e (assuming higher sensitivity) would only be very likely at the $1–2\varepsilon_{RMS}$ thresholds and have even odds at the $3\varepsilon_{RMS}$ level. Given that the AOD and r_e perturbations we estimated are both within $1\varepsilon_{RMS}$ of their

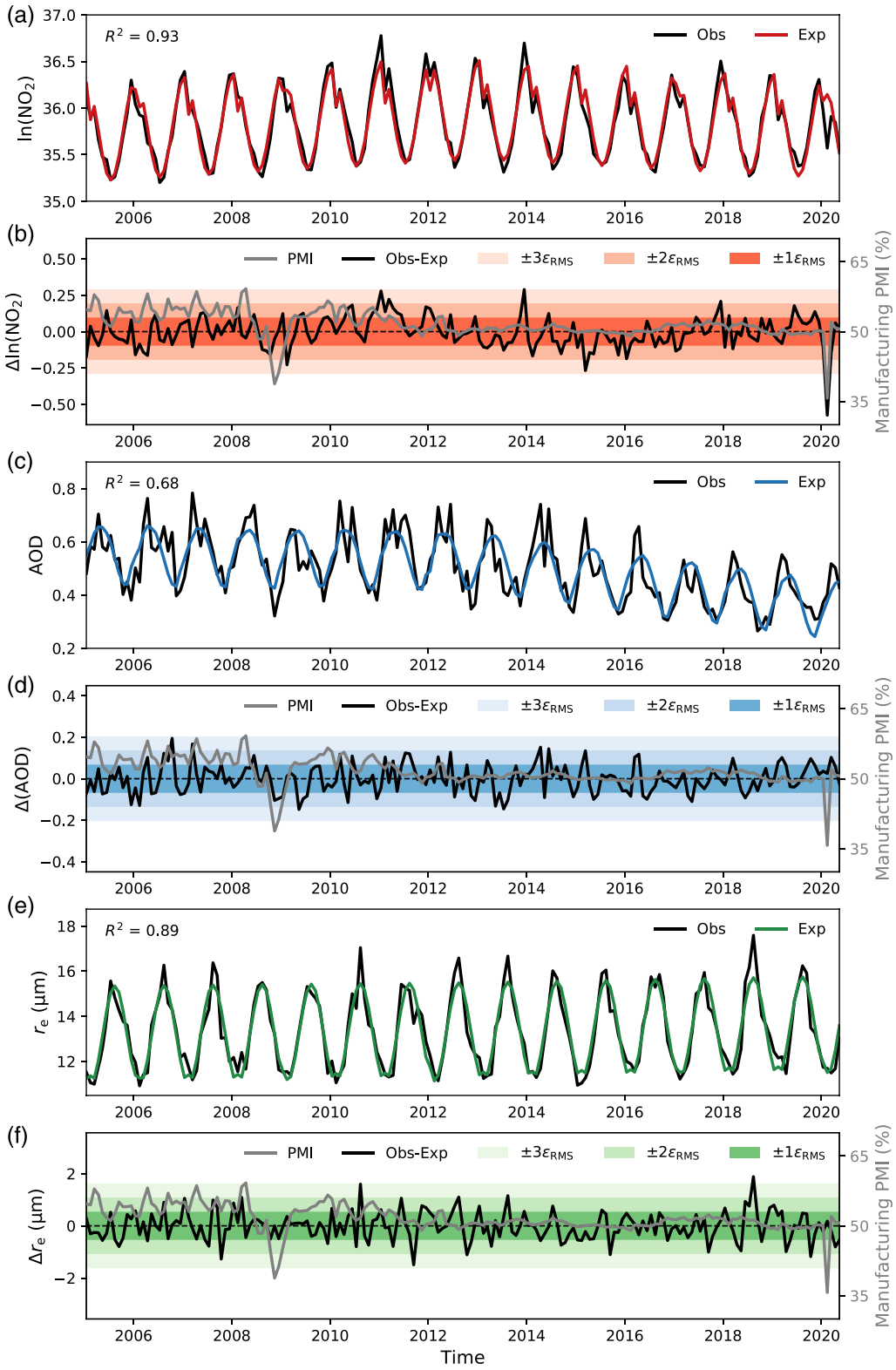

Figure 3. Time series of observed (Obs) and expected (Exp) values and their differences for (a, b) ln(NO_2), (c, d) AOD, and (e, f) r_e, as averaged over the boxes in Figure 2. Manufacturing PMI is shown for reference.

expected values, this analysis suggests that aerosol reductions during the February 2020 lockdown period were unlikely to have exceeded ~20%.

4. Factors Influencing Pollution Changes During the February 2020 Shutdown

4.1. Meteorology

Meteorology is an important driver of changes in pollution concentrations (de Foy et al., 2016; P. Wang et al., 2020; Zhai et al., 2019; Zhang et al., 2019). To assess the effects of meteorology on our results, we create a second linear regression model as follows:

$$Y_{\mathrm{met}}(t,\phi,\lambda) = c_0(\phi,\lambda) + c_{\mathrm{pre}}(\phi,\lambda)P_{\mathrm{pre}}(t) + c_{\mathrm{post}}(\phi,\lambda)P_{\mathrm{post}}(t) + c_{\mathrm{CNY}}(\phi,\lambda)H_{\mathrm{CNY}}(t) + c_{\mathrm{T}}(\phi,\lambda)T_{2\mathrm{M}}(t,\phi,\lambda) \quad (5)$$
$$+ c_{\mathrm{q_v}}(\phi,\lambda)Q_{2\mathrm{M}}(t,\phi,\lambda) + c_{\mathrm{u}}(\phi,\lambda)U_{10\mathrm{M}}(t,\phi,\lambda) + c_{\mathrm{v}}(\phi,\lambda)V_{10\mathrm{M}}(t,\phi,\lambda),$$

where Y_{met} is the geophysical variable of interest, the terms relating to policy-driven trends and holiday effects are the same as for the model in Equation 1, and the idealized seasonal cycle has been replaced by the meteorological terms $T_{2\mathrm{M}}$ for 2-m air temperature, $Q_{2\mathrm{M}}$ for 2-m specific humidity, and $U_{10\mathrm{M}}$ and $V_{10\mathrm{M}}$ for 10-m zonal and meridional winds, respectively. All meteorological variables are standardized by subtracting the 2005–2019 mean from each monthly value and dividing by the 2005–2019 standard deviation. Figure S8 shows maps of regression diagnostics (R^2, $\varepsilon_{\mathrm{RMS}}$, and N), and Figures S9–S11 show maps of the intercept and regression coefficients for $\ln(\mathrm{NO_2})$, AOD, and r_{e}, respectively.

Figure S12 shows time series of the regionally averaged results, which are overall similar to those in Figure 3.

The differences between the model described by Equation 1 and the observations can be interpreted as being due to a combination of meteorology and emissions (including emissions-concentrations-chemistry interactions), whereas the difference between the model described by Equation 5 and the observations can be interpreted as being due to emissions alone. (Of course, there also may be other factors that have not been accounted for or meteorological effects not captured by the linear model.) The effect of meteorology can be estimated in two ways: as the difference between the expectations between the two models or as the difference between the model described by Equation 5 and the same model with the meteorological factors set to their mean values for a given month. Similarly, the (linear) contribution of individual meteorological variables can be estimated as the difference between the model described by Equation 5 and that model with the meteorological variable of interest set to its monthly mean value.

Figure S13 shows the decomposition of emission and meteorology effects using this framework for February 2020. Meteorology alone would have led to a ~10% decrease in $\mathrm{NO_2}$, driven mostly by temperature, followed by humidity. The emissions effect alone would have led to a ~50% decrease. In contrast, meteorology is estimated to have increased AOD by ~5%. Meteorological anomalies during February 2020 are shown in Figure S14. Conditions were warmer and wetter than average, corresponding with increased chemical sinks of $\mathrm{NO_2}$ but more potential for secondary production of aerosol (Le et al., 2020).

4.2. Emissions

Another explanation for the different NO_x and aerosol responses is that economic sectors that disproportionately emit one or the other pollutant may have been impacted differently by the shutdown. Figures 1c and 1d show changes in passenger transportation, energy generation, and iron and steel production from 2005 to 2020. Figure S15 includes a variety of other economic subsectors tracked by the National Bureau of Statistics of China. Passenger transportation, in particular, was devastated by the shutdown. In contrast, total January–February power generation was down ~10% (similar to 2008–2009), implying a decrease of ~20% in February alone. Heavy industries like steel production (slightly up) were comparatively unaffected, with the remainder of the economy somewhere in between.

Different reporting metrics were chosen based on data quality and availability. For a more directly comparable (but temporally limited) perspective, Figure S16 shows the change in January–March production between 2020 and 2019 for each subsector.

Anthropogenic emissions of NO_x (E_{NO_x}), $\mathrm{PM}_{2.5}$ ($E_{\mathrm{PM}_{2.5}}$), and $\mathrm{SO_2}$ ($E_{\mathrm{SO_2}}$) for the year 2015 from EDGAR are combined to create aggregate "transportation" and "industry and power" sectors, with the remainder

lumped into an "other" category primarily consisting of agriculture and waste management. (See supporting information Tables S1–S3 for the specific breakdown of the transportation, industry and power, and "other" sectors, respectively, by IPCC 2006, code.) Figure S17 shows maps of the contributions of the three pollutants by economic sector. Transportation is a major source of NO_x pollution, comparable to the industry and power sectors, whereas the industry and power sectors dominate emissions of primary $PM_{2.5}$ and SO_2 (a major aerosol precursor). Supporting information Tables S1–S3 provide sums of annual emissions in 2015 over eastern China for each sector grouping. The transportation sector accounts for 26.2% of all NO_x emissions but only 4.7% of $PM_{2.5}$ and 3.6% of SO_2 emissions (Table S1), while the industry and power sectors account for 72.3% of NO_x, 92.8% of $PM_{2.5}$, and 95.1% of SO_2 emissions (Table S2). Given that decreases in NO_x, $PM_{2.5}$, and SO_2 since 2015 have been driven primarily by regulations targeting the industrial sector (Zhang et al., 2019), it is likely that the transportation sector comprised a greater share of total NO_x emissions in 2020 than in 2015.

The ~50% decline in NO_2 due to emissions can be mostly explained by a dramatic fall in transportation emissions paired with a 10–20% reduction in energy and industrial sources. A ~20% decline in aerosol emissions would likely go undetected by our method (Figure S7). At the same time, this analysis suggests that the estimated ~40% decline in coal burning during the Chinese lockdown period from Le Quéré et al. (2020) is unrealistically high, both because electrical and thermal power declined by only ~20% at peak and because a ~40% decline in aerosol emissions should have been detectable, at least at the less stringent thresholds. The Chinese coal data in that study come from a private industry analysis of several power plants, which may not have been representative of the national response. However, given that reductions in ground transportation dominate their analysis as well, even halving the industrial change estimates would not substantially change their results (e.g., the peak global decline on 7 April 2020 would fall ~10%, from ~17 to ~15 $MtCO_2$/day).

One caveat about our aerosol estimates is that we assume that the significant aerosol reductions between 2013 and 2017 continued during 2018–2020. If we instead were to freeze P_{post} at its 2017 value (assume no further progress), the observed AOD would have been 10–20% below its expected value. Our analysis is consistent with no aerosol change, a moderate decrease, or, as discussed below, a moderate decrease in emissions compensated by increased secondary production.

4.3. Chemistry

As a further complication, meteorological anomalies, emissions changes, and their interactions influenced atmospheric chemistry and therefore pollution concentrations in February 2020.

During the winter, the atmospheric lifetime of NO_x (~1 day) over eastern China decreases with decreasing emissions as higher ozone concentrations allow for more loss via reaction with hydrogen oxide radicals (HO_x) during the day and via hydrolysis of N_2O_5 (an important NO_x reservoir) within aerosols at night (Shah et al., 2020). We may therefore expect decreases in NO_2 concentrations to exceed reductions in NO_x emissions.

$PM_{2.5}$ concentrations may either increase or decrease as a response to a NO_x decline depending on its magnitude and background concentrations (Zhao et al., 2017). The increase in O_3 as NO_x emissions fall (Shi & Brasseur, 2020) increases HO_x concentrations and thus the atmospheric oxidizing capacity, which could further reduce NO_2 but facilitate secondary aerosol formation (X. Huang, Ding, Gao, et al., 2020). This in combination with the relatively warm and wet February 2020 meteorological conditions offers a compelling explanation for the apparent increase in aerosol surrounding Beijing (X. Huang, Ding, Gao, et al., 2020; Le et al., 2020; P. Wang et al., 2020), although the effect appears to be weaker in other regions, perhaps due to differences in background conditions. However, regional aerosol changes are not necessarily independent as transport and aerosol-boundary layer interactions can lead to a complex interplay in pollution levels between regions (Chang et al., 2020; X. Huang et al., 2020).

To assess potential changes in aerosol composition and size distribution, we analyze ω_0 and α using the model described by Equation 1. Figure S18 shows time series of observed and expected values, and Figure S19 shows maps of the February 2020 anomalies. Since 2013 there has been a trend toward higher ω_0 (less absorption) and lower α (coarser size distribution), which is reversed during February 2020 (more

absorbing and finer aerosol). The anomalies in February 2020 are similar to those in December 2019, however, so it is not clear that these anomalies can be attributed to shutdown effects.

5. Conclusions

Despite unprecedented declines in economic activity and NO_x emissions during the February 2020 coronavirus shutdown in China, we find no detectable perturbation in aerosol and related cloud properties. The severe curtailment of passenger transportation (a disproportionate NO_x source) but comparatively muted changes in power generation and heavy industry (disproportionate $PM_{2.5}$ and SO_2 sources), along with meteorology and complex chemical interactions, help explain this discrepancy.

Further study of the environmental consequences of COVID-19 is warranted, not least because potential links between long-term and short-term air quality and vulnerability to the disease remain unresolved (Contini & Costabile, 2020). There is some evidence that short-term exposure to air pollution increased the case fatality rate of the 2002–2003 Severe acute respiratory syndrome outbreak in several Chinese cities (Cui et al., 2003), which raises the possibility of feedbacks between containment measures that reduce pollution and population-level resilience. Additionally, dramatically reduced transportation sector emissions without similar changes in other sectors could represent a plausible future emissions mix if widespread electrification of transportation is adopted but other sectors do not adopt similar pollution mitigation measures.

Data Availability Statement

OMI/Aura and MODIS/Aqua Level 3 gridded data and MERRA-2 meteorological reanalysis data are publicly available from NASA's Goddard Earth Sciences Data and Information Services Center (https://disc.gsfc.nasa.gov/). Various economic statistics from the People's Republic of China are publicly available from the National Bureau of Statistics of China (http://www.stats.gov.cn/english/). EDGAR's annual sector-specific grid maps are publicly available from the European Commission's Joint Research Center (https://edgar.jrc.ec.europa.eu/overview.php?v=50_AP; https://data.europa.eu/doi/10.2904/JRC_DATASET_EDGAR).

Acknowledgments

M. S. D. was supported by NASA Headquarters under the NASA Earth and Space Science Fellowship Program Grant NNX-80NSSC17K0404. We thank Kyle Armour, Fiona Lo, Daniel McCoy, Joel Thornton, and Casey Wall for helpful discussion and Aijun Ding and Jean-François Müller for constructive reviews that helped improve the manuscript.

References

Ackerman, A. S., Kirkpatrick, M. P., Stevens, D. E., & Toon, O. B. (2004). The impact of humidity above stratiform clouds on indirect aerosol climate forcing. *Nature*, *432*(7020), 1014–1017. https://doi.org/10.1038/nature03174

Albrecht, B. A. (1989). Aerosols, cloud microphysics, and fractional cloudiness. *Science*, *245*(4923), 1227–1230. https://doi.org/10.1126/science.245.4923.1227

Atkinson, R. W., Butland, B. K., Anderson, H. R., & Maynard, R. L. (2018). Long-term concentrations of nitrogen dioxide and mortality: A meta-analysis of cohort studies. *Epidemiology*, *29*(4), 460–472. https://doi.org/10.1097/EDE.0000000000000847

Bauwens, M., Compernolle, S., Stavrakou, T., Müller, J. F., Gent, J., Eskes, H., et al. (2020). Impact of coronavirus outbreak on NO_2 pollution assessed using TROPOMI and OMI observations. *Geophysical Research Letters*, *47*, e2020GL087978. https://doi.org/10.1029/2020GL087978

Bellouin, N., Quaas, J., Gryspeerdt, E., Kinne, S., Stier, P., Watson-Parris, D., et al. (2020). Bounding global aerosol radiative forcing of climate change. *Reviews of Geophysics*, *58*, e2019RG000660. https://doi.org/10.1029/2019RG000660

Bennartz, R., Fan, J., Rausch, J., Leung, L. R., & Heidinger, A. K. (2011). Pollution from China increases cloud droplet number, suppresses rain over the East China Sea. *Geophysical Research Letters*, *38*, L09704. https://doi.org/10.1029/2011gl047235

Burnett, R., Chen, H., Szyszkowicz, M., Fann, N., Hubbell, B., Pope, C. A. III, et al. (2018). Global estimates of mortality associated with long-term exposure to outdoor fine particulate matter. *Proceedings of the National Academy of Sciences*, *115*(38), 9592–9597. https://doi.org/10.1073/pnas.1803222115

Cermak, J., & Knutti, R. (2009). Beijing Olympics as an aerosol field experiment. *Geophysical Research Letters*, *36*, L10806. https://doi.org/10.1029/2009GL038572

Chang, Y., Huang, R. J., Ge, X., Huang, X., Hu, J., Duan, Y., et al. (2020). Puzzling haze events in China during the coronavirus (COVID-19) shutdown. *Geophysical Research Letters*, *47*, e2020GL088533. https://doi.org/10.1029/2020GL088533

Contini, D., & Costabile, F. (2020). Does air pollution influence COVID-19 outbreaks? *Atmosphere*, *11*(4), 377–381. https://doi.org/10.3390/atmos11040377

Crippa, M., Guizzardi, D., Muntean, M., Schaaf, E., Dentener, F., van Aardenne, J. A., et al. (2018). Gridded emissions of air pollutants for the period 1970–2012 within EDGAR v4.3.2. *Earth System Science Data*, *10*(4), 1987–2013. https://doi.org/10.5194/essd-10-1987-2018

Crippa, M., Solazzo, E., Huang, G., Guizzardi, D., Koffi, E., Muntean, M., et al. (2020). High resolution temporal profiles in the Emissions Database for Global Atmospheric Research. *Scientific Data*, *7*(1), 121–137. https://doi.org/10.1038/s41597-020-0462-2

Cui, Y., Zhang, Z.-F., Froines, J., Zhao, J., Wang, H., Yu, S.-Z., & Detels, R. (2003). Air pollution and case fatality of SARS in the People's Republic of China: An ecologic study. *Environmental Health*, *2*(1), 15–19. https://doi.org/10.1186/1476-069X-2-15

de Foy, B., Lu, Z., & Streets, D. G. (2016). Satellite NO_2 retrievals suggest China has exceeded its NO_x reduction goals from the twelfth Five-Year Plan. *Scientific Reports*, *6*(1), 35,912–35,920. https://doi.org/10.1038/srep35912

Ding, A., Huang, X., Nie, W., Chi, X., Xu, Z., Zheng, L., et al. (2019). Significant reduction of PM2.5 in eastern China due to regional-scale emission control: Evidence from SORPES in 2011–2018. *Atmospheric Chemistry and Physics*, *19*(18), 11,791–11,801. https://doi.org/10.5194/acp-19-11791-2019

Ding, J., van Der, A. R. J., Mijling, B., Levelt, P. F., & Hao, N. (2015). NO_x emission estimates during the 2014 Youth Olympic Games in Nanjing. *Atmospheric Chemistry and Physics*, *15*(16), 9399–9412. https://doi.org/10.5194/acp-15-9399-2015

Gelaro, R., McCarty, W., Suárez, M. J., Todling, R., Molod, A., Takacs, L., et al. (2017). The Modern-Era Retrospective Analysis for Research and Applications, version 2 (MERRA-2). *Journal of Climate*, *30*(14), 5419–5454. https://doi.org/10.1175/JCLI-D-16-0758.1

Gryspeerdt, E., Quaas, J., & Bellouin, N. (2016). Constraining the aerosol influence on cloud fraction. *Journal of Geophysical Research: Atmospheres*, *121*, 3566–3583. https://doi.org/10.1002/2015JD023744

Hao, N., Valks, P., Loyola, D., Cheng, Y. F., & Zimmer, W. (2011). Space-based measurements of air quality during the World Expo 2010 in Shanghai. *Environmental Research Letters*, *6*(4), 044004. https://doi.org/10.1088/1748-9326/6/4/044004

Harris, E. S. (1991). Tracking the economy with the purchasing managers' index. *Federal Reserve Bank of New York Quarterly Review, Autumn*, *16*, 61–69.

Hsu, N. C., Jeong, M. J., Bettenhausen, C., Sayer, A. M., Hansell, R., Seftor, C. S., et al. (2013). Enhanced Deep Blue aerosol retrieval algorithm: The second generation. *Journal of Geophysical Research: Atmospheres*, *118*, 9296–9315. https://doi.org/10.1002/jgrd.50712

Huang, R., Zhang, Y., Bozzetti, C., Ho, K. F., Cao, J. J., Han, Y., et al. (2014). High secondary aerosol contribution to particulate pollution during haze events in China. *Nature*, *514*(7521), 218–222. https://doi.org/10.1038/nature13774

Huang, X., Ding, A., Gao, J., Zheng, B., Zhou, D., Qi, X., et al. (2020). Enhanced secondary pollution offset reduction of primary emissions during COVID-19 lockdown in China. *National Science Review*, nwaa137. https://doi.org/10.1093/nsr/nwaa137

Huang, X., Ding, A., Wang, Z., Ding, K., Gao, J., Chai, F., & Fu, C. (2020). Amplified transboundary transport of haze by aerosol–boundary layer interaction in China. *Nature Geoscience*, *13*(6), 428–434. https://doi.org/10.1038/s41561-020-0583-4

Hubanks, P. A., Platnick, S., King, M. D., & Ridgway, W. (2019). MODIS Atmosphere L3 Gridded product. Algorithm theoretical basis document (ATBD) & users guide. https://modis-atmosphere.gsfc.nasa.gov/sites/default/files/ModAtmo/L3_ATBD_C6_C61_2019_02_20.pdf

IPCC (2006). 2006 IPCC guidelines for national greenhouse gas inventories. In H. S. Eggleston, L. Buendia, K. Miwa, N. T., & T. K (Eds.), *Prepared by the National Greenhouse Gas Inventories Programme*. Japan: IGES.

Jiang, Q., Sun, Y. L., Wang, Z., & Yin, Y. (2015). Aerosol composition and sources during the Chinese Spring Festival: Fireworks, secondary aerosol, and holiday effects. *Atmospheric Chemistry and Physics*, *15*(11), 6023–6034. https://doi.org/10.5194/acp-15-6023-2015

Jin, Y., Andersson, H., & Zhang, S. (2016). Air pollution control policies in China: A retrospective and prospects. *International Journal of Environmental Research and Public Health*, *13*(12), 1219–1240. https://doi.org/10.3390/ijerph13121219

Krotkov, N. A., Lamsal, L. N., Celarier, E. A., Swartz, W. H., Marchenko, S. V., Bucsela, E. J., et al. (2017). The version 3 OMI NO_2 standard product. *Atmospheric Measurement Techniques*, *10*(9), 3133–3149. https://doi.org/10.5194/amt-10-3133-2017

Krotkov, N. A., Lamsal, L. N., Marchenko, S. V., Celarier, E. A., Bucsela, E. J., Swartz, W. H., et al. (2019). OMI/Aura NO_2 cloud-screened total and tropospheric column L3 global gridded 0.25 degree x 0.25 degree v3, NASA Goddard Space Flight Center, Goddard Earth Sciences Data and Information Services Center (GES DISC). https://doi.org/10.5067/Aura/OMI/DATA3007, Accessed: June 1, 2020.

Krotkov, N. A., Li, C., & Leonard, P. (2015). OMI/Aura sulfur dioxide (SO_2) total column L3 1 day best pixel in 0.25 degree x 0.25 degree v3, Greenbelt, MD, USA, Goddard Earth Sciences Data and Information Services Center (GES DISC). https://doi.org/10.5067/Aura/OMI/DATA3008, Accessed: June 1, 2020.

Krotkov, N. A., McLinden, C. A., Li, C., Lamsal, L. N., Celarier, E. A., Marchenko, S. V., et al. (2016). Aura OMI observations of regional SO_2 and NO_2 pollution changes from 2005 to 2015. *Atmospheric Chemistry and Physics*, *16*(7), 4605–4629. https://doi.org/10.5194/acp-16-4605-2016

Le Quéré, C., Jackson, R. B., Jones, M. W., Smith, A. J. P., Abernethy, S., Andrew, R. M., et al. (2020). Temporary reduction in daily global CO_2 emissions during the COVID-19 forced confinement. *Nature Climate Change*, *10*(7), 647–653. https://doi.org/10.1038/s41558-020-0797-x

Le, T., Wang, Y., Liu, L., Yang, J., Yung, Y. L., Li, G., & Seinfeld, J. H. (2020). Unexpected air pollution with marked emission reductions during the COVID-19 outbreak in China. *Science*, *369*, eabb7431. https://doi.org/10.1126/science.abb7431

Levelt, P. F., Joiner, J., Tamminen, J., Veefkind, J. P., Bhartia, P. K., Stein Zweers, D. C., et al. (2018). The Ozone Monitoring Instrument: Overview of 14 years in space. *Atmospheric Chemistry and Physics*, *18*(8), 5699–5745. https://doi.org/10.5194/acp-18-5699-2018

Liu, F., Page, A., Strode, S. A., Yoshida, Y., Choi, S., Zheng, B., et al. (2020). Abrupt decline in tropospheric nitrogen dioxide over China after the outbreak of COVID-19. *Science Advances*, *6*(28), eabc2992. https://doi.org/10.1126/sciadv.abc2992

Liu, F., Zhang, Q., van Der, A. R. J., Zheng, B., Tong, D., Yan, L., et al. (2016). Recent reduction in NO_x emissions over China: Synthesis of satellite observations and emission inventories. *Environmental Research Letters*, *11*, 114002. https://doi.org/10.1088/1748-9326/11/11/114002

Maier, B. F., & Brockmann, D. (2020). Effective containment explains subexponential growth in recent confirmed COVID-19 cases in China. *Science*, *368*(6492), 742–746. https://doi.org/10.1126/science.abb4557

Malavelle, F. F., Haywood, J. M., Jones, A., Gettelman, A., Clarisse, L., Bauduin, S., et al. (2017). Strong constraints on aerosol-cloud interactions from volcanic eruptions. *Nature*, *546*(7659), 485–491. https://doi.org/10.1038/nature22974

McCoy, D. T., Bender, F. A. M., Grosvenor, D. P., Mohrmann, J. K., Hartmann, D. L., Wood, R., & Field, P. R. (2018). Predicting decadal trends in cloud droplet number concentration using reanalysis and satellite data. *Atmospheric Chemistry and Physics*, *18*(3), 2035–2047. https://doi.org/10.5194/acp-18-2035-2018

Myhre, G., Shindell, D., Bréon, F.-M., Collins, W., Fuglestvedt, J., Huang, J., et al. (2013). Chapter 8: Anthropogenic and natural radiative forcing. In T. F. Stocker, et al. (Eds.), *Climate change 2013: The physical science basis. Contribution of Working Group I to the Fifth Assessment Report of the Intergovernmental Panel on Climate Change* (pp. 659–740). Cambridge, UK and New York, NY: Cambridge University Press.

Parkinson, C. L. (2003). Aqua: An Earth-observing satellite mission to examine water and other climate variables. *IEEE Transactions on Geoscience and Remote Sensing*, *41*(2), 173–183. https://doi.org/10.1109/TGRS.2002.808319

Pedregosa, F., Varoquaux, G., Gramfort, A., Michel, V., Thirion, B., Grisel, O., et al. (2011). Scikit-learn: Machine learning in Python. *Journal of Machine Learning Research*, *12*, 2825–2830.

Platnick, S., Meyer, K. G., King, M. D., Wind, G., Amarasinghe, N., Marchant, B., et al. (2017). The MODIS cloud optical and microphysical products: Collection 6 updates and examples from Terra and Aqua. *IEEE Transactions on Geoscience and Remote Sensing*, *55*(1), 502–525. https://doi.org/10.1109/TGRS.2016.2610522

Sayer, A. M., Hsu, N. C., Lee, J., Kim, W. V., & Dutcher, S. T. (2019). Validation, stability, and consistency of MODIS Collection 6.1 and VIIRS version 1 Deep Blue aerosol data over land. *Journal of Geophysical Research: Atmospheres*, *124*, 4658–4688. https://doi.org/10.1029/2018JD029598

Schoeberl, M. R., Douglass, A. R., Hilsenrath, E., Bhartia, P. K., Beer, R., Waters, J. W., et al. (2006). Overview of the EOS aura mission. *IEEE Transactions on Geoscience and Remote Sensing*, *44*(5), 1066–1074. https://doi.org/10.1109/TGRS.2005.861950

Shah, V., Jacob, D. J., Li, K., Silvern, R. F., Zhai, S., Liu, M., et al. (2020). Effect of changing NO_x lifetime on the seasonality and long-term trends of satellite-observed tropospheric NO_2 columns over China. *Atmospheric Chemistry and Physics*, *20*(3), 1483–1495. https://doi.org/10.5194/acp-20-1483-2020

Shi, X., & Brasseur, G. P. (2020). The response in air quality to the reduction of Chinese economic activities during the COVID-19 outbreak. *Geophysical Research Letters*, *47*, e2020GL088070. https://doi.org/10.1029/2020GL088070

Silver, B., Reddington, C. L., Arnold, S. R., & Spracklen, D. V. (2018). Substantial changes in air pollution across China during 2015–2017. *Environmental Research Letters*, *13*(11), 114012. https://doi.org/10.1088/1748-9326/aae718

Stevens, B., & Feingold, G. (2009). Untangling aerosol effects on clouds and precipitation in a buffered system. *Nature*, *461*(7264), 607–613. https://doi.org/10.1038/nature08281

Storelvmo, T. (2017). Aerosol effects on climate via mixed-phase and ice clouds. *Annual Review of Earth and Planetary Sciences*, *45*(1), 199–222. https://doi.org/10.1146/annurev-earth-060115-012240

Tan, P.-H., Chou, C., Liang, J.-Y., Chou, C. C. K., & Shiu, C.-J. (2009). Air pollution "holiday effect" resulting from the Chinese New Year. *Atmospheric Environment*, *43*(13), 2114–2124. https://doi.org/10.1016/j.atmosenv.2009.01.037

Tian, H., Liu, Y., Li, Y., Wu, C.-H., Chen, B., Kraemer, M. U. G., et al. (2020). An investigation of transmission control measures during the first 50 days of the COVID-19 epidemic in China. *Science*, *368*(6491), 638–642. https://doi.org/10.1126/science.abb6105

Toll, V., Christensen, M., Quaas, J., & Bellouin, N. (2019). Weak average liquid-cloud-water response to anthropogenic aerosols. *Nature*, *572*(7767), 51–55. https://doi.org/10.1038/s41586-019-1423-9

Twomey, S. (1977). The influence of pollution on the shortwave albedo of clouds. *Journal of the Atmospheric Sciences*, *34*(7), 1149–1152. https://doi.org/10.1175/1520-0469%281977%29034%3C1149%3ATIOPOT%3E2.0.CO%3B2

van der A, R. J., Mijling, B., Ding, J., Koukouli, M. E., Liu, F., Li, Q., et al. (2017). Cleaning up the air: Effectiveness of air quality policy for SO_2 and NO_x emissions in China. *Atmospheric Chemistry and Physics*, *17*(3), 1775–1789. https://doi.org/10.5194/acp-17-1775-2017

Wang, C., Horby, P. W., Hayden, F. G., & Gao, G. F. (2020). A novel coronavirus outbreak of global health concern. *The Lancet*, *395*(10223), 470–473. https://doi.org/10.1016/S0140-6736(20)30185-9

Wang, P., Chen, K., Zhu, S., Wang, P., & Zhang, H. (2020). Severe air pollution events not avoided by reduced anthropogenic activities during COVID-19 outbreak. *Resources, Conservation, & Recycling*, *158*, 104814. https://doi.org/10.1016/j.resconrec.2020.104814

Witte, J. C., Schoeberl, M. R., Douglass, A. R., Gleason, J. F., Krotkov, N. A., Gille, J. C., et al. (2009). Satellite observations of changes in air quality during the 2008 Beijing Olympics and Paralympics. *Geophysical Research Letters*, *36*, L17803. https://doi.org/10.1029/2009GL039236

Zhai, S., Jacob, D. J., Wang, X., Shen, L., Li, K., Zhang, Y., et al. (2019). Fine particulate matter ($PM_{2.5}$) trends in China, 2013–2018: Separating contributions from anthropogenic emissions and meteorology. *Atmospheric Chemistry and Physics*, *19*(16), 11,031–11,041. https://doi.org/10.5194/acp-19-11031-2019

Zhang, Q., Zheng, Y., Tong, D., Shao, M., Wang, S., Zhang, Y., et al. (2019). Drivers of improved $PM_{2.5}$ air quality in China from 2013 to 2017. *Proceedings of the National Academy of Sciences*, *116*(49), 24,463–24,469. https://doi.org/10.1073/pnas.1907956116

Zhao, B., Wu, W., Wang, S., Xing, J., Chang, X., Liou, K.-N., et al. (2017). A modeling study of the nonlinear response of fine particles to air pollutant emissions in the Beijing–Tianjin–Hebei region. *Atmospheric Chemistry and Physics*, *17*(19), 12,031–12,050. https://doi.org/10.5194/acp-17-12031-2017

Zheng, B., Tong, D., Li, M., Liu, F., Hong, C., Geng, G., et al. (2018). Trends in China's anthropogenic emissions since 2010 as the consequence of clean air actions. *Atmospheric Chemistry and Physics*, *18*(19), 14,095–14,111. https://doi.org/10.5194/acp-18-14095-2018

Zheng, G., Duan, F. K., Su, H., Ma, Y. L., Cheng, Y., Zheng, B., et al. (2015). Exploring the severe winter haze in Beijing: The impact of synoptic weather, regional transport and heterogeneous reactions. *Atmospheric Chemistry and Physics*, *15*(6), 2969–2983. https://doi.org/10.5194/acp-15-2969-2015

Zheng, Y., Xue, T., Zhang, Q., Geng, G., Tong, D., Li, X., & He, K. (2017). Air quality improvements and health benefits from China's clean air action since 2013. *Environmental Research Letters*, *12*(11), 114020. https://doi.org/10.1088/1748-9326/aa8a32